# A secreted MMP is required for reepithelialization during wound healing

Laura J. Stevens[a] and Andrea Page-McCaw[a,b]
[a]Department of Cell and Developmental Biology and Program in Developmental Biology and [b]Department of Cancer Biology, Vanderbilt University Medical Center, Nashville, TN 37232

**ABSTRACT** **Matrix metalloproteinases (MMPs) are extracellular proteases highly expressed at wound sites. However, the precise function of MMPs during reepithelialization in vivo has been elusive in mammalian models because of the high level of redundancy among the 24 mammalian MMPs. For this reason we used *Drosophila melanogaster*, whose genome encodes only two MMPs—one secreted type (*Mmp1*) and one membrane-anchored type (*Mmp2*)—to study the function and regulation of the secreted class of MMPs in vivo. In the absence of redundancy, we found that the *Drosophila* secreted MMP, Mmp1, is required in the epidermis to facilitate reepithelialization by remodeling the basement membrane, promoting cell elongation and actin cytoskeletal reorganization, and activating extracellular signal-regulated kinase signaling. In addition, we report that the jun N-terminal kinase (JNK) pathway upregulates *Mmp1* expression after wounding, but that Mmp1 is expressed independent of the JNK pathway in unwounded epidermis. When the JNK pathway is ectopically activated to overexpress Mmp1, the rate of healing is accelerated in an Mmp1-dependent manner. A primary function of Mmp1, under the control of the JNK pathway, is to promote basement membrane repair, which in turn may permit cell migration and the restoration of a continuous tissue.**

**Monitoring Editor**
Marcos Gonzalez-Gaitan
University of Geneva

Received: Sep 2, 2011
Revised: Dec 8, 2011
Accepted: Jan 10, 2012

## INTRODUCTION

Healing a human skin wound requires a complex interplay of cells and extracellular matrix (ECM) within a tissue architecture that directs and restricts molecular interactions. In the hemostasis phase, platelets form a plug, which is replaced by a temporary fibrin matrix; in the inflammatory phase, white blood cells neutralize pathogens and phagocytose cell and ECM debris; in the reepithelialization stage, epidermal epithelial cells migrate into the wound bed and collagen-based scar tissue replaces the fibrin matrix; and in the resolution phase, white blood cells are cleared and provisional ECM is replaced (Singer and Clark, 1999; Gurtner *et al.*, 2008; Shaw and Martin, 2009; Goldberg and Diegelmann, 2010). These stages are controlled by many growth factors and extracellular signals, including platelet-derived growth factor, epidermal growth factor, tumor necrosis factor α (TNFα), transforming growth factor β, and insulin-like growth factor. In healthy individuals small wounds heal without intervention, but clinical wound-healing challenges remain for surgical patients, diabetic patients, and burn victims. Pathologies of wound healing can be roughly grouped into two categories: excessive wound healing, leading to fibrotic scarring, and incomplete wound healing, leading to ulcers and persistent inflammation (Goldberg and Diegelmann, 2010).

Matrix metalloproteinases (MMPs) comprise a large family of extracellular proteases, at least 10 of which are up-regulated during wound healing by epidermal, dermal, fibroblast, or blood cells in mammals (reviewed by Gill and Parks, 2008). MMPs can be subdivided into two classes: secreted MMPs (17 mammalian family members) and membrane-anchored MMPs (seven mammalian family members). Their endogenous inhibitors are tissue inhibitors of metalloproteinases (TIMPs), which sterically hinder the active site in a one-to-one stoichiometry (Gomis-Ruth *et al.*, 1997). In vitro and in cell culture, MMPs are capable of cleaving most ECM components

This article was published online ahead of print in MBoC in Press (http://www.molbiolcell.org/cgi/doi/10.1091/mbc.E11-09-0745) on January 19, 2012.

Address correspondence to: Andrea Page-McCaw (andrea.page-mccaw@vanderbilt.edu).

Abbreviations used: DAPI, 4′,6-diamidino-2-phenylindole; dsRNA, double-stranded RNA; ECM, extracellular matrix; ERK, extracellular signal-related kinase; GFP, green fluorescent protein; GPI, glycophosphatidylinositol; JNK, Jun N-terminal kinase; MMP, matrix metalloproteinase; RNAi, RNA interference; SEM, standard error of the mean; TIMP, tissue inhibitor of metalloproteinases; TNF, tumor necrosis factor.

and proteolytically modifying many signaling molecules important for wound healing (Gearing *et al.*, 1995; Levi *et al.*, 1996; Suzuki *et al.*, 1997; Bergers *et al.*, 2000; Yu and Stamenkovic, 2000; Egeblad and Werb, 2002; Li *et al.*, 2002; Koshikawa *et al.*, 2004; Mott and Werb, 2004; Parks *et al.*, 2004; Gill and Parks, 2008; Tholozan *et al.*, 2007; Rebustini *et al.*, 2009). MMPs are widely considered to be proinflammatory during the wound-healing process because of the high levels of MMP expression in chronic wounds (Menke *et al.*, 2007; Schultz and Wysocki, 2009; Goldberg and Diegelmann, 2010). However, MMPs may have larger roles, as they sit at the nexus of inflammation, ECM remodeling, and cell signaling (reviewed in Parks *et al.*, 2004). Mouse MMP knockouts have limited utility in defining MMP functions because of redundancy within the MMP family (Page-McCaw *et al.*, 2007). Knockout mice for each of four secreted MMPs (*MMP-3, MMP-8, MMP-9*, and *MMP-13*) display a mild delay in closing excisional wounds, indicating that MMPs have a functional role in wound healing. *MMP-3* (stromelysin-1) mutants have defects in wound contraction (Bullard *et al.*, 1999); *MMP-8* mutants have prolonged inflammation (Gutierrez-Fernandez *et al.*, 2007); *MMP-9* and *MMP-13* mutants have delays in epithelial migration (Hattori *et al.*, 2009; Kyriakides *et al.*, 2009). These mild phenotypes probably belie the role of MMPs in wound healing, as the vertebrate MMP family displays significant redundancy. The ~24 mammalian MMPs have overlapping substrate specificity and expression patterns (Egeblad and Werb, 2002). Indeed, MMP redundancy in wounding has been reported: *MMP-9/-13* double mutants have longer wound-healing delays than the single mutants (Hattori *et al.*, 2009), and yet even these mice still have a large number of intact MMP genes that may be masking other MMP wound-healing functions. This genetic redundancy clouds a mechanistic understanding of wound healing in vivo.

*Drosophila* is an established model system for wound healing (Wood *et al.*, 2002; Galko and Krasnow, 2004), and in *Drosophila* there are only two MMPs: one secreted (DmMmp1) and one membrane anchored (DmMmp2; Llano *et al.*, 2000, 2002; Page-McCaw *et al.*, 2003). In addition, the *Drosophila* MMPs are inhibited by a single endogenous TIMP (DmTimp; Godenschwege *et al.*, 2000; Wei *et al.*, 2003), in contrast to the four TIMPs in mammals. This simplicity allows us to identify the roles of the secreted and membrane-anchored MMPs as a class in vivo, including their tissue sources and regulatory mechanisms. *Drosophila* wound healing involves the same wound-healing phases as for vertebrates (hemostasis, inflammation, reepithelialization, and resolution; Galko and Krasnow, 2004), including the migratory reepithelialization phase. We report here that *Mmp1* and *Mmp2* are each required for reepithelialization during wound healing, as puncture wounds remain open in the mutants. Focusing on the secreted MMP—Mmp1—we report that it facilitates reepithelialization by promoting ECM assembly, cell elongation, actin cytoskeletal reorganization, and extracellular signal-regulated kinase (ERK) activation. The wound-induced up-regulation of Mmp1 is controlled by jun N-terminal kinase (JNK), and when JNK is ectopically activated by TNF to produce high levels of Mmp1, wound closure is accelerated in an Mmp1-dependent manner.

## RESULTS

### Both *Drosophila* MMPs are required for wound healing

Mmp1, the secreted *Drosophila* MMP, is required for developmental tissue remodeling during tracheal growth and metamorphosis (Srivastava *et al.*, 2007; Glasheen *et al.*, 2009, 2010). We asked whether Mmp1 is required for tissue remodeling during wound healing of the larval epidermis. Larval epidermis is a monolayer squamous epithelium that is protected on the apical side by a chitinous cuticle and overlies a basal basement membrane (Martinez Arias, 1993). Most larval epidermal cells are highly polyploid and incapable of proliferation (Smith and Orr-Weaver, 1991). To assess wound healing, we punctured larval epidermis in the wild type and in *Mmp1*-null mutants with a fine needle, using the procedure of Galko and Krasnow (2004). We used third-instar animals; $Mmp1^{2}$-null mutants die during a prolonged third instar and almost never enter metamorphosis (Page-McCaw *et al.*, 2003). After puncture, the animals were allowed a recovery period for healing, and then we dissected, fixed, and stained the epidermis with anti-FasIII and 4′,6-diamidino-2-phenylindole (DAPI) to visualize cell borders and nuclei. In wild-type larvae 5 h after wounding, epidermal cells at the wound edge had elongated and begun spreading into the wound; by 14 h wounds had typically closed, often forming syncytia over the center of the wound, as previously reported (Galko and Krasnow, 2004). Assessing wound closure by location of nuclei and cell borders, we found that 79% of wild-type animals closed their wounds by 14 h (n = 19; Figure 1, A and E).

In contrast, reepithelialization failed to occur in 100% of wounded *Mmp1*-null animals, both homozygous null $Mmp1^{2}$ larvae and transheterozygous null $Mmp1^{2/Q112*}$, demonstrating specificity for *Mmp1* (Figure 1, B and E). The *Mmp1* wounds gapped open by 1 h (Figure 1G) and remained larger than the original puncture (Figure 1, F and G). These were not simply delays in wounding, as *Mmp1* wounds never closed: even at 50 h postwounding, the rare surviving *Mmp1* mutants still had open wounds (n = 2), whereas all wild-type wounds were closed (n = 4).

There are only two MMPs in *Drosophila*, so we asked whether the predicted GPI-anchored MMP, *Mmp2*, was also required for wound healing. In both $Mmp2^{W307*}$ and $Mmp2^{W307*/Df(2R)Uba1\text{-}Mmp2}$ animals, wounds failed to close (Figure 1, C, E, and F). We overexpressed the catalytic inhibitor Timp throughout the larval epidermis using the *A58-GAL4* driver (Galko and Krasnow, 2004), and the expression of this endogenous inhibitor recapitulated the failure of reepithelialization in the MMP mutants with large wounds (Figure 1, D–F). Thus each *Drosophila* MMP is required for wound closure in a nonredundant manner.

To test for redundant roles, we administered puncture wounds to double-mutant *Mmp2 Mmp1* animals. Both single-MMP mutants had an incompletely penetrant clotting defect, such that many of the animals died after puncturing. In double mutants, the clotting defect was pronounced and fully penetrant: all the animals bled out and died shortly after wounding, indicating that they have clot formation defects (n = 84). Thus *Drosophila* MMPs appear to act redundantly in the hemostasis phase of wound healing, but each is required for reepithelialization. We focus primarily on Mmp1 in this article.

### *Mmp1* is required in the epidermis for reepithelialization

Epidermal wound healing involves the coordination of at least two different tissue types: epidermal epithelial cells and hemocytes (innate immune cells of the blood). To elucidate which tissue(s) require *Mmp1* during reepithelialization, we knocked down *Mmp1* using an inducible RNA interference (RNAi) targeting construct (Uhlirova and Bohmann, 2006) under the control of tissue-specific GAL4 drivers *A58-GAL4* (epidermis) and *He-GAL4* (hemocytes). By 18 h postwounding, wounds closed in 86% of wild-type animals (Figure 2, A and E). Similar to the whole-animal *Mmp1* mutants (Figure 1B), when *Mmp1* was knocked down specifically in the epidermis (*A58>Mmp1-dsRNA*), wounds remained open in 100% of animals 18 h postwounding (Figure 2, C and E), with an average wound area that was

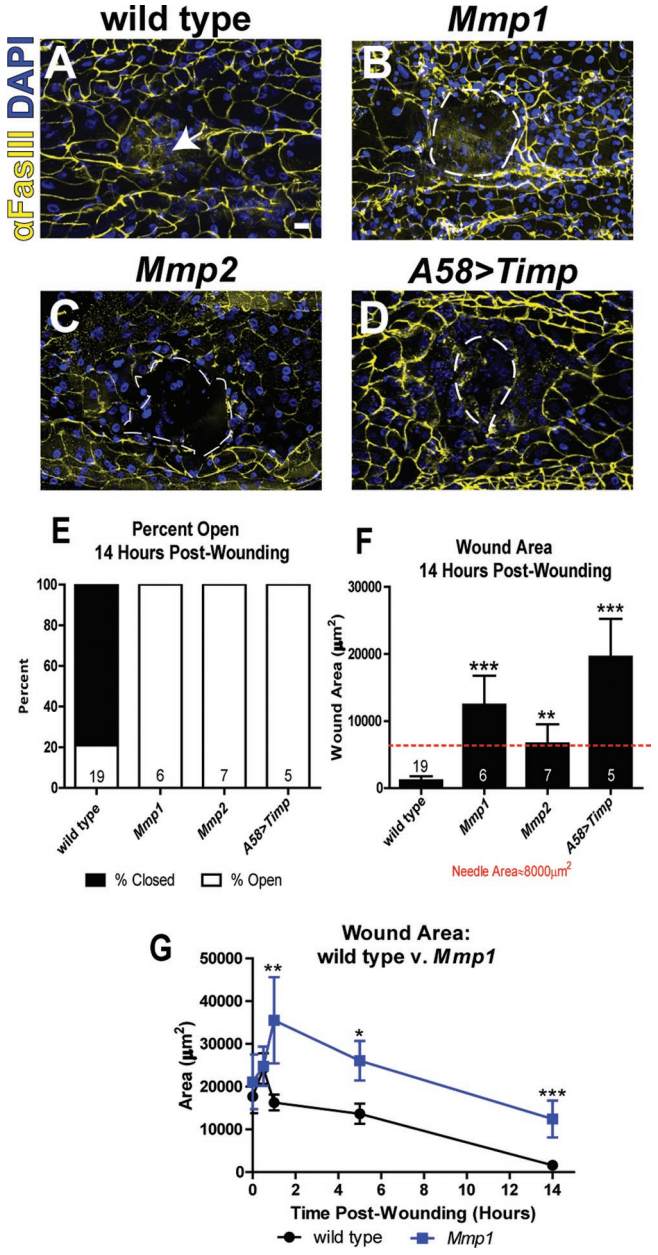


FIGURE 1: Each *Drosophila* MMP is required for reepithelialization. (A–D) Wounded larval epidermis 14 h postwounding from indicated genotypes. Anti-FasIII (yellow) labels cell borders, and DAPI (blue) labels the nuclei. The white arrow (A) indicates the center of the closed wound, and the white, dashed lines outline open wounds (B–D). Scale bar in A represents 20 μm for A–D. (E) Percentage of wounds open vs. closed 14 h postwounding. The numbers on each bar (E, F) indicate the number of animals for each sample set. (F) Mean wound area 14 h postwounding (including all wounds, open and closed). The red, dashed line represents the area of the needle used to induce wounds (~8000 μm$^2$). Mutants are significantly different from wild type, as calculated by *t* test: *Mmp1* (p = 0.0004), *Mmp2* (p = 0.011), *A58>Timp* (p < 0.0001). (G) Graph of wound area over time in wild type (black line) and *Mmp1* mutants (blue line). At 1 h (*Mmp1*, n = 4; wild type, n = 21), 5 h (*Mmp1*, n = 14; wild type, n = 23), and 14 h (*Mmp1*, n = 6; wild type, n = 19) postwounding, mutant wounds are significantly larger than wild type (p = 0.003, 0.032, and 0.0001, respectively). There is no significant difference in wound area between *Mmp1* mutants and wild type at 0 h (*Mmp1*, n = 4; wild type, n = 8) and 0.5 h (*Mmp1*, n = 5; wild type, n = 15) postwounding. Error bars (F, G) represent SEM. See *Materials and Methods* for alleles used.

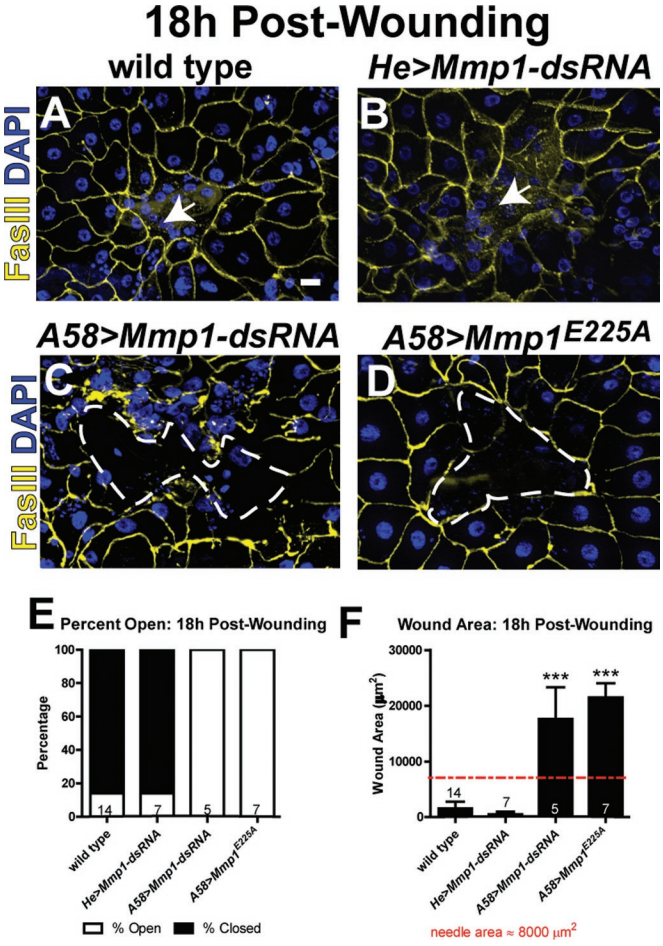


FIGURE 2: Epidermal *Mmp1* is required for reepithelialization. (A–D) Wounded epidermis 18 h postwounding from the designated genotypes. The white arrows (A, B) point to the region of the closed wounds. White, dashed lines (C, D) outline open wounds. Scale bar in A represents 20 μm for A–D. (E) Graph showing percentage of wounds open vs. closed 18 h postwounding in each genotype. (F) Graph of the wound area 18 h postwounding. The numbers above the *x*-axis indicate the number of animals examined for each group. Wound areas in *A58>Mmp1-dsRNA* (p = 0.0007) and *A58>Mmp1$^{E225A}$* (p < 0.0001) mutants are significantly larger than in wild type by Student's *t* test. Error bars (F) show SEM.

significantly larger than that for wild type (Figure 2F). In contrast, when *Mmp1* was knocked down in hemocytes *(He>Mmp1*-dsRNA), healing was similar to that in wild type (Figure 2, B, E, and F). To ensure specificity of the RNAi, we used an *Mmp1-dsRNA* line targeting another region of the transcript (from the VDRC), with similar results (data not shown). An anti-Mmp1 Western blot confirmed that both lines reduced protein levels, with the Bohmann line more effective (Supplemental Figure S2). These results demonstrate that *Mmp1* expression in the epidermis is required for reepithelialization.

To test whether the catalytic activity of Mmp1 was required for wound closure, we expressed in the epidermis a catalytically inactive Mmp1, *UAS-Mmp1$^{E225A}$*, which harbors an alanine mutation at a conserved glutamic acid in the active site and acts as a dominant negative (Zhang *et al.*, 2006; Glasheen *et al.*, 2009). In animals expressing *Mmp1$^{E225A}$* in the epidermis, wounds remained open in 100% of the animals tested 18 h postwounding (Figure 2, D and E), with an average wound area that is similar to that for the RNAi-mediated knockdown of Mmp1 (Figure 2F).

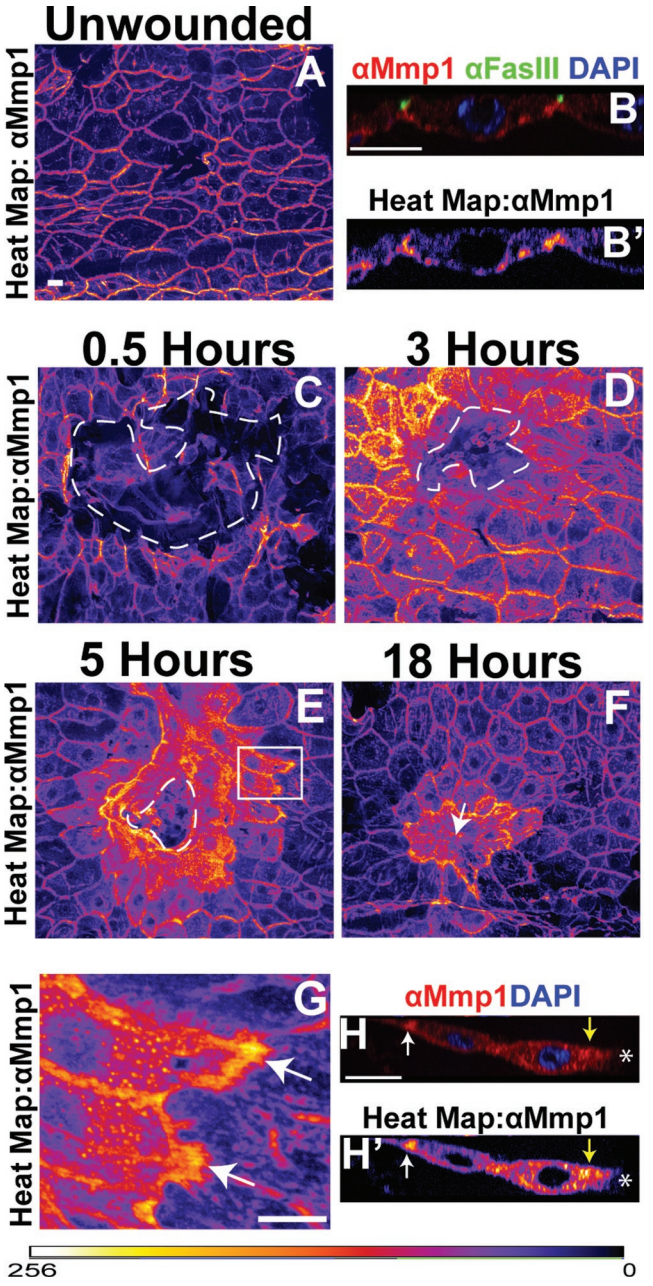


FIGURE 3: Mmp1 is upregulated at the wound site. (A) Heat map showing Mmp1 localization in unwounded larval epidermis, pseudocolored based on pixel intensity, intensity scale for A–G displayed at bottom of figure. (B, B′) X-Z images of epidermis showing anti-Mmp1 staining (red in B, heat map in B′), the cell border marker FasIII (green in B), and DAPI (blue in B). Apical is up. (C–F) Heat maps showing anti-Mmp1 staining after wounding. The white, dashed lines in C–E outline the wound bed, and the white arrow in F indicates the closed wound. Comparison of Mmp1 intensity levels can be made between A and C–F, as images were taken at matched exposure settings. (C) Mmp1 0.5 h postwounding. (D) Mmp1 3 h postwounding. (E) Mmp1 5 h postwounding. (F) Mmp1 18 h postwounding. (G) Close-up of epidermal cells near the leading edge 5 h postwounding (white box in E) with white arrows pointing to distal-edge accumulation of Mmp1. (H, H′) X-Z images of Mmp1 (red in H, heat map in H′) and DAPI (blue in H) in two epidermal cells at the leading edge of a 5-h wound. Apical is up. White asterisk indicates the wound bed. Yellow arrows designate proximal Mmp1 accumulation around the leading edge, and white arrow indicates distal Mmp1 accumulation. All scale bars, 20 μm. Scale bar in A also for C–F.

Our results indicate that Mmp1 catalytic activity is required for reepithelialization.

### Mmp1 is up-regulated in the epidermis in response to wounding

To test whether there is a local response to wounding, we analyzed wound-induced Mmp1 expression changes in the epidermis. The dynamic range of Mmp1 expression is so large that we visualized Mmp1 expression changes by pseudocoloring anti-Mmp1 images based on pixel intensity to generate heat maps (see Figure 3 and *Materials and Methods*). Using specific monoclonal antibodies that recognize the catalytic domain of Mmp1 (Page-McCaw *et al.*, 2003; Glasheen *et al.*, 2010), we found that Mmp1 was expressed at low levels throughout the unwounded epidermis (Figure 3, A and B). In X-Y projections, Mmp1 appeared localized to the cell–cell borders (Figure 3A), but in X-Z projections, it was clear that Mmp1 also lines the basal surface of the epidermal cells, where it could come in contact with the basement membrane (Figure 3, B and B′). At ½ h after wounding, Mmp1 expression had not changed at the wound site (Figure 3C), but by 3 h after wounding, Mmp1 was up-regulated in the epidermal cells specifically around the wound site (Figure 3D), with no detectable changes in expression in cells more than four to five cell diameters away from the wound. Maximal up-regulation was observed at 5 h postwounding (Figure 3E and data not shown). Elevated Mmp1 levels persisted in the syncytia and surrounding epithelial cells even after the wound was closed (Figure 3F). Mmp1 was also upregulated in pinch wounds in which the cuticle was not broken (Supplemental Figure S1), suggesting that Mmp1 up-regulation is triggered by damage rather than by the introduction of pathogens. We found that Mmp1 is generally upregulated in a gradient highest in the cells at the wound margin (Figure 3, D and E). Although Mmp1 is up-regulated throughout these cells (Figure 3, E–G), there is an unexpected accumulation of Mmp1 at the distal edge (Figure 3, E, white box, G, H, and H′; white arrows indicate distal accumulation), as well as high levels of Mmp1 proximal to the wound margin (Figure 3, H and H′, yellow arrow).

### *Mmp1* promotes assembly or maintenance of the basement membrane

To heal mammalian puncture wounds, two kinds of ECM must be repaired—stromal ECM and the basement membrane. Although insects use an exoskeleton in place of most stromal ECM, the basement membrane of *Drosophila* is a collagen IV–containing matrix highly homologous to that of vertebrates (Hynes and Zhao, 2000). *Drosophila* has two conserved subfamilies of collagen IV—α1-like, encoded by *cg25C*, and α2-like, encoded by *vkg* (Yasothornsrikul *et al.*, 1997)—and both are found in basement membranes (Murray *et al.*, 1995; Noselli, 1998; Pastor-Pareja and Xu, 2011). Because MMPs derive their name from their ability to degrade ECM, we compared the basement membrane during wound healing in wild-type and *Mmp1*-mutant larvae. We used a Vkg–green fluorescent protein (GFP) protein trap expressed under its endogenous promoter to visualize the basement membrane (Morin *et al.*, 2001). By 1 h postwounding in wild-type animals there was no detectable Vkg-GFP accumulation along the wound edge (data not shown); however, by 5 h postwounding in wild-type larvae there was dramatic Vkg-GFP accumulation at or directly in front of the leading edge (n = 6; Figure 4, A, A′, and C). In the *Mmp1*-null mutants, there was no accumulation of Vkg-GFP at the leading edge (n = 8; Figure 4, B, B′, and D). Of note, Mmp1 is expressed heavily around the leading edge by 5 h after wounding (Figure 3, E and G) at the site where Vkg is assembled. Our data suggest that *Mmp1* promotes the assembly of

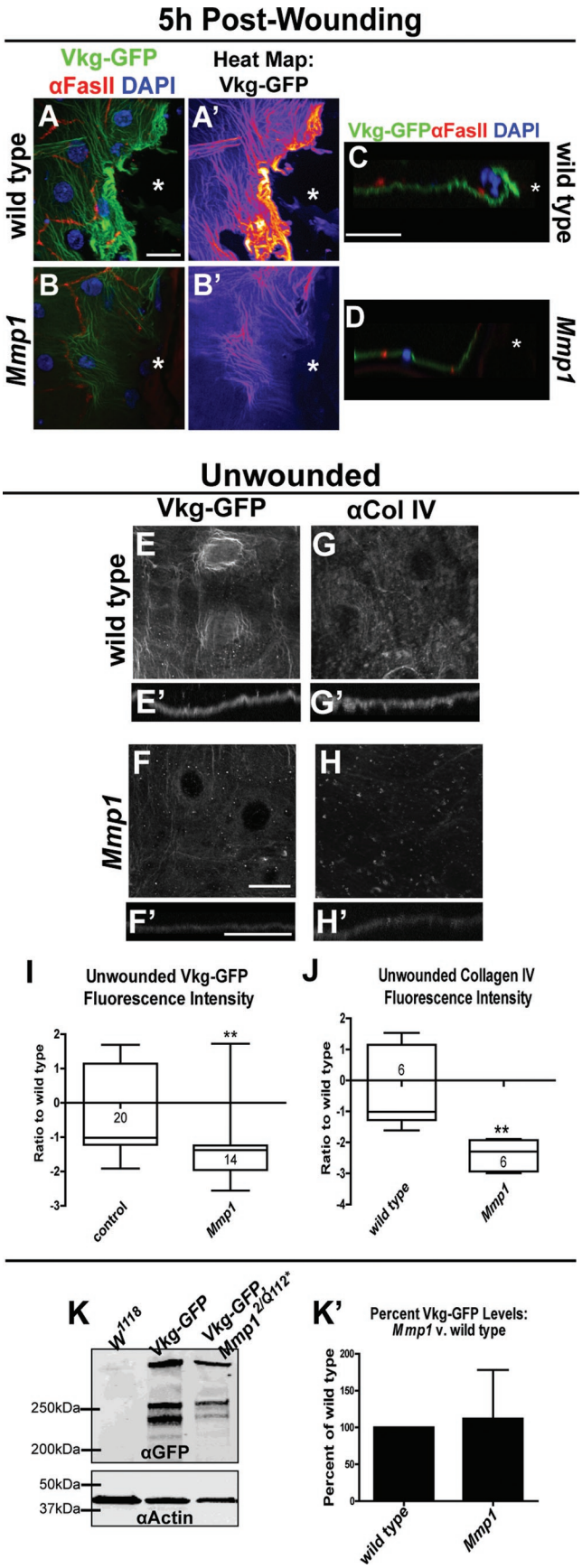


FIGURE 4: Mmp1 is required for ECM remodeling and maintenance. (A, B) Vkg-GFP at wound margin 5 h postwounding (green), with nuclei (blue, DAPI) and cell borders (red, anti-FasIII) in *Vkg-GFP/+* (A; n = 6 animals) and in *Vkg-GFP* $Mmp1^{Q112*}/Mmp1^{2}$ (B; n = 8 animals). White asterisk indicates wound bed. (A′, B′) Heat maps of Vkg-GFP from A and B. (C, D) X-Z image of Vkg-GFP (green), FasIII (red), and DAPI (blue) at the wound edge 5 h postwounding in control (C) and *Mmp1* mutants (D). White asterisks designate wound beds. (E, F) Vkg-GFP localization in unwounded epidermis in control (E) and $Mmp1^{2/Q112*}$ mutants (F). (E′, F′) X-Z image of Vkg-GFP in unwounded control (E′) and *Mmp1* mutants (F′). (G, H) Anti–collagen IV (Cg25C) staining in unwounded epidermis in wild type (G) and in *Mmp1* mutants (H); n = 6 animals for each genotype. (G′, H′) X-Z images of anti–collagen IV staining in wild type (G′) and *Mmp1* mutants (H′). All scale bars, 20 μm; scale bar in A for A–D; scale bar in F for E–H; scale bar in F′ for E′–H′. (I, J) Box-and-whiskers plot of Vkg-GFP intensity or collagen IV staining intensity (J) in unwounded basement membrane in control and *Mmp1* mutants. Numbers in the boxes on the graph indicate the number of animals measured. By Student's *t* test, Vkg-GFP intensity (p = 0.0051) and anti–collagen IV staining intensity (p = 0.0054) are significantly lower in *Mmp1* mutants relative to wild type. (K) Western blot of anti-GFP in unwounded whole *Vkg-GFP/+* and *Vkg-GFP* $Mmp1^{Q112*}/Mmp1^{2}$ larvae, with anti-actin as a loading control. (K′) Quantification of three Western blots (as in K), showing no significant difference between Vkg-GFP protein levels in whole *Mmp1*-mutant larvae vs. wild type by paired *t* test (p = 0.87). The fluorescence intensity of the bands was normalized to the loading control. Error bars represent SEM.

collagen IV at wound sites rather than promotes widespread degradation of collagen IV. It is possible that without new basement membrane, *Mmp1* mutant wounds are unable to close because the epidermal cells lack a substrate on which to migrate.

Because *Mmp1* is needed for wound-induced basement membrane assembly, we asked whether it is necessary for basement membrane maintenance in unwounded epidermis, especially considering that Mmp1 protein is localized to the basal side of these cells (Figure 3B). We used the Vkg-GFP protein trap to analyze baseline collagen IV levels and structure in unwounded tissue (Figure 4, E and F). In wild-type basement membrane underlying unwounded epidermis, Vkg-GFP appeared as a fibrous mesh, slightly concentrated around the cell nuclei (Figure 4, E and E′). In *Mmp1* mutants, the overall Vkg-GFP fibrous pattern was similar to wild type, but the intensity was significantly lower than wild type (Figure 4, F, F′, and I), as scored in seven blind experiments. As an independent confirmation of collagen IV localization in the unwounded basement membrane, we stained epidermal samples with a monoclonal antibody raised against cg25C (collagen IV α1); this antibody has been used previously for immunostaining (Murray *et al.*, 1995). We again observed reduced levels of collagen IV in the *Mmp1* unwounded epidermal basement membrane (Figure 4, H, H′, and J) compared with wild type (Figure 4, G, G′, and J). These data suggest that either *Mmp1* is necessary for assembling collagen IV into the basement membrane or *Mmp1* is required for the expression or stability of collagen IV proteins. To test the latter hypothesis, we compared Vkg-GFP protein levels in whole larvae on Western blots probed for GFP (Figure 4K). We found no significant differences in Vkg-GFP levels between wild type and *Mmp1* mutants (Figure 4, K and K′). Our data suggest that Mmp1 is required to facilitate Vkg-GFP deposition into the basement membrane both at wound sites and during normal growth but not for overall Vkg-GFP expression or stability.

### *Mmp1* is required for migration after wounding

Cell migration is required to close wounds, so we asked whether cells at the leading edge of *Mmp1* mutant wounds were able to migrate. As cells migrate, they elongate in the direction of migration

(reviewed in Mogilner and Keren, 2009). We measured the aspect ratio of epidermal cells at the leading edge of the wound site (see *Materials and Methods*), comparing cell shape in healing wounds to initial cell shape in wounds that were immediately fixed after puncture, reasoning that the cell elongation represents a measure of migration. In wild-type wounds, we found that cell aspect ratios appeared to increase gradually over time but that by 5 h after wounding, cells had clearly elongated (Supplemental Figure S3C). By 5 h postwounding, wild-type leading-edge cells were almost twice as elongated as they were immediately postwounding (Figure 5, A, A′, and C).

In contrast, leading edge cells failed to elongate by 5 h in *Mmp1* mutants (Figure 5, B, B′, and C), and the aspect ratio remained fairly constant after wounding (Supplemental Figure S3D). In these mutants, cells maintained the aspect ratio that they took on immediately after injury. We noticed that *Mmp1* epidermal cells are smaller than wild-type cells (Figure 5, A and B, and Supplemental Figure S3, A and B), which might be secondary to the pronounced tracheal defects in the mutant that cause hypoxia (Beaucher *et al.*, 2007; Glasheen *et al.*, 2010). Epidermal cells knocked down for *Mmp1* (*A58>Mmp1-dsRNA*; Figure 5C) did not exhibit marked changes in cell size, and these cells also failed to elongate after wounding (Figure 5D), demonstrating that *Mmp1* is specifically required for cell elongation and migration. Similarly, when we overexpressed *Timp* in the epidermis, leading-edge cells failed to elongate (Figure 5D). These data demonstrate that *Mmp1* in the epidermis is required for cells to elongate, the first step of migration.

Another characteristic of migrating cells is the presence of actin-rich projections in the direction of migration (reviewed in Mogilner and Keren, 2009). As a second indicator of cell migration, we analyzed wound-induced actin changes in leading-edge epidermal cells using an Actin5C-GFP fusion protein (Verkhusha *et al.*, 1999) expressed specifically in the epidermis with *A58-GAL4*. In wild-type tissue 1 h after wounding we observed actin accumulation along the proximal side of leading edge cells, along with small, thin, actin-rich projections extending into the wound bed (data not shown). By 5 h postwounding, wild-type cells had dense actin mesh along the proximal side of the leading edge cells with long, thick, actin-rich projections extending into the wound bed (Figure 5E), suggesting that these cells were actively migrating. In contrast, in *Mmp1* mutants 5 h postwounding we observed actin accumulation in stress fibers along the leading edge but no projections extending into the wound bed (Figure 5F), suggesting that leading-edge cells in *Mmp1* mutants do not migrate to close the wound.

One possible explanation for the lack of cell elongation in *Mmp1* mutants is that Mmp1 may be required to release the adhesion of cells from the ECM. In cell culture models, integrins on the distal edges of migrating cells are released from the basement membrane, allowing cells to progress forward, and there are reports of MMPs cleaving integrins (Vaisar *et al.*, 2009; Pal-Ghosh *et al.*, 2011). We examined βPS integrin localization at wild-type wounds by antibody staining, and we found that Mmp1 protein colocalized with βPS integrin at the distal edges of cells at the wound (Supplemental Figure S4). Although this colocalization suggested that Mmp1 may have a role in releasing β-integrins after wounding, we did not observe changes to integrin localization in our fixed wild-type samples at any time points during reepithelialization (data not shown). Similarly, no changes in β-integrin staining were evident in *Mmp1*-mutant wounds relative to wild-type wounds (data not shown). Although these negative results do not rule out the hypothesis that Mmp1 releases integrin-based adhesion, it seems unlikely that a failure to release adhesion at the distal edge would result in the observed failure of cell elongation (Figure 5, A–D); instead, persistent integrin adhesion at the distal edge would be expected to result in perpetually elongated cells that are nonmotile, a phenotype not observed.

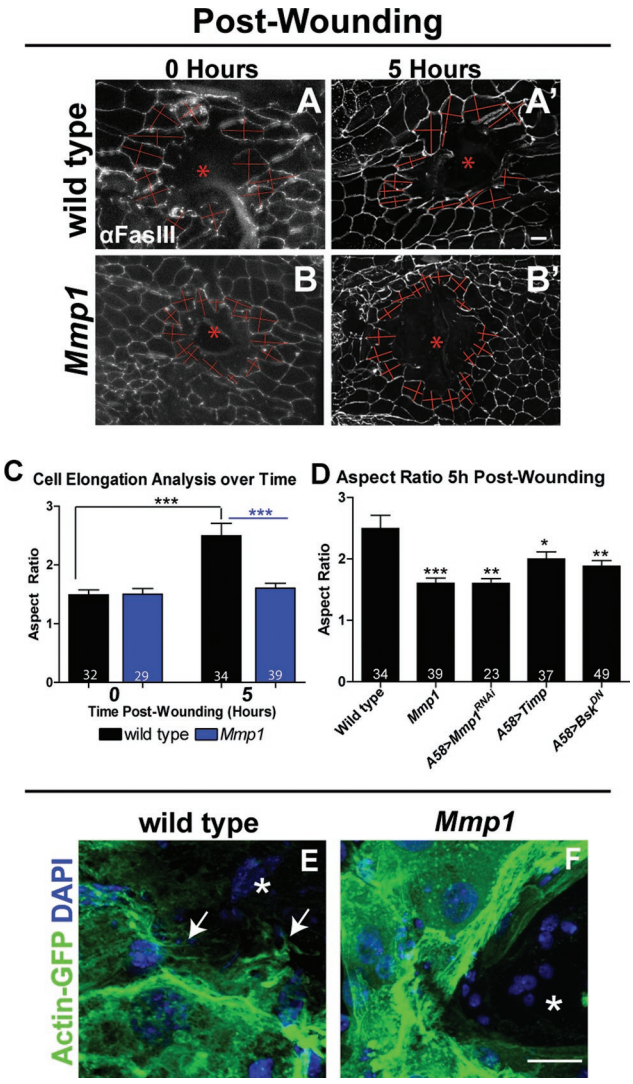


FIGURE 5: *Mmp1* is required for leading-edge cell migration. (A, B) Aspect ratios of wild-type (A, A′) and *Mmp1* (B, B′) leading-edge cells were calculated by measuring perpendicular axes (shown in red) at 0 h (A, B) and 5 h (A′,B′) after wounding. See *Materials and Methods* for details. (C) Aspect ratio analysis for wild type (black bars) and *Mmp1* mutants (blue bars). Black stars indicate that wild-type cells at 5 h are significantly different from wild-type cells at 0 h postwounding ($p < 0.0001$) by Student's *t* test. Blue stars show that *Mmp1*-mutant cells are significantly different from wild type at 5 h ($p = 0.0001$) postwounding by Student's *t* test. There is no significant difference in aspect ratio between wild-type and *Mmp1* mutant cells 0 h postwounding, and similarly cells in *Mmp1* mutants show no significant change in aspect ratio between 0 and 5 h after wounding. (D) Aspect ratio 5 h postwounding. Leading-edge cells in *Mmp1* mutants ($p = 0.0001$), *A58>Mmp1-dsRNA* ($p = 0.0015$), *A58>Timp* ($p = 0.041$), and *A58>Bsk*$^{DN}$ ($p = 0.0043$) are significantly less elongated than wild type at 5 h postwounding. Numbers in the base of each bar (C, D) denote the number of cells measured. Error bars represent SEM. (E, F) Actin-GFP localization around control *A58>Actin-GFP* (E) and mutant *Mmp1*$^{2}$ *A58>actin-GFP* (F) wounds (n = 3 for each genotype). White arrows (E) indicate actin-rich protrusions into the wound bed. Asterisk indicates a wound bed (A, B, E, and F). All scale bars, 20 μm; A and B′ scale bar in A′; E and F scale bar in F.

### Mmp1 promotes ERK activation

In addition to functioning to remodel ECM, MMPs are also known to process components of signaling pathways, both activating and inactivating them (reviewed by Page-McCaw *et al.*, 2007; Gill and Parks, 2008). In mammalian cell culture studies, ERK activation is necessary to induce epithelial cell motility and invasiveness (Matsubayashi *et al.*, 2004; Doehn *et al.*, 2009). It has been reported that ERK, a kinase that mediates receptor tyrosine kinase signaling, is activated in larval epidermal wounds (Wu *et al.*, 2009). To determine whether *Mmp1* is required for signaling through receptor tyrosine kinase pathways, we examined the activation of ERK (encoded by *rolled*) in *Mmp1* mutants compared with wild type. On pathway activation, ERK is phosphorylated on two residues (called dpERK) and is translocated to the nucleus, where it can be detected by a diphospho-ERK–specific antibody (Gabay *et al.*, 1997; Helman and Paroush, 2010). To examine ERK activation in leading edge nuclei, we blindly outlined the nuclei around the wound using only DAPI as a guide and then measured the ERK staining within the marked areas (see *Materials and Methods*). In wild-type animals, we found that dpERK activation is nearly undetectable in unwounded epidermis and increases modestly at 0.5 and 1 h after wounding; however, by 3 and 5 h after wounding, dpERK levels are much greater in nuclei at the leading edge of wounds (Supplemental Figure S5 and Figure 6, A–A″). In contrast, in *Mmp1*-mutant animals, ERK activation does not change appreciably after wounding (Figure 6, B and D). Similarly, in epidermal knockdowns of *Mmp1* (*A58>Mmp1-dsRNA*), dpERK activation is significantly decreased after wounding (Figure 6, C and D), although not as completely as in the *Mmp1*-null animals, perhaps because of the residual leakiness of the knockdown (Supplemental Figure S2) or because of Mmp1 contributions from other unaffected tissues. Our data demonstrate that *Mmp1* is required to promote ERK signaling in epidermal cells after wounding.

### *Mmp1* is regulated by JNK signaling during wound healing

Another pathway known to be required for wound healing is the JNK pathway (Ramet *et al.*, 2002; Galko and Krasnow, 2004; Wu *et al.*, 2009). Previous studies showed that Mmp1 is regulated by JNK signaling during tumor invasion and wing disk eversion (Uhlirova and Bohmann, 2006; Srivastava *et al.*, 2007). We asked whether JNK signaling regulates Mmp1 activity during reepithelialization by using a JNK (*Bsk*) dominant-negative construct (*UAS-Bsk$^{DN}$*) to interfere with JNK signaling specifically in the epidermis (*A58>Bsk$^{DN}$*). In unwounded tissue, there was no apparent difference in Mmp1 expression or localization in wild type compared with *A58>Bsk$^{DN}$* (compare Figure 7, A and C). After wounding, however, Mmp1 was not up-regulated in the epidermis of *A58>Bsk$^{DN}$* mutants as it was in wild type (compare Figure 7, B and D). Furthermore, the reepithelialization defects seen in the *Mmp1* mutants are also observed in the *A58>Bsk$^{DN}$* mutants, including cell elongation failures (Figure 5D) and wound closure failures (Galko and Krasnow, 2004; our data not shown).

Ectopic up-regulation of the JNK pathway resulted in the up-regulation of Mmp1. Previous studies showed that TNF stimulates JNK activation in mammalian cells and in *Drosophila* (Brenner *et al.*, 1989; Igaki *et al.*, 2009). We hyperstimulated the JNK pathway by overexpressing *Drosophila* TNF, *eiger* (*egr*), in the epidermis (*A58>egr*). Mmp1 expression in unwounded *A58>egr* epidermis was similar to wild type (compare Figure 7, A and E). In contrast, 5 h after wounding *A58>egr* epidermis, we observed dramatic Mmp1 up-regulation not only in the epidermal cells at the wound site, but also extending to epidermal cells approximately five cell

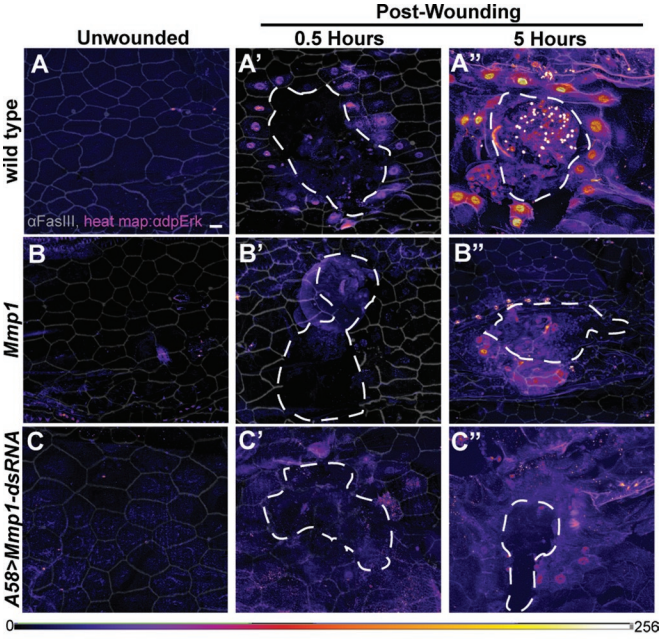


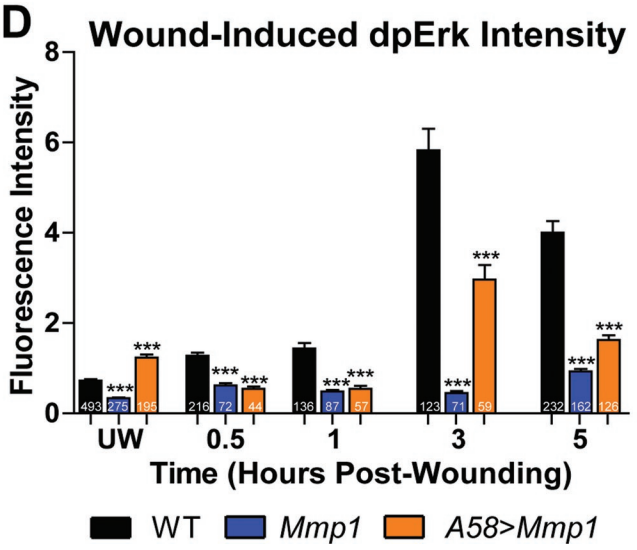


FIGURE 6: Mmp1 promotes wound-induced ERK activation. (A–C) Heat maps of anti-dpERK staining (color scale below C) in the indicated genotypes in unwounded condition (A–C) and 0.5 h (A′–C′) or 5 h (A″–C″) postwounding (n ≥ 4 for all genotypes and time points). The cell border marker FasIII (gray lines) is overlaid onto each image (A–C″) to outline cells. White, dashed lines (A′–C′ and A″–C″) outline the wound bed. Scale bar in A represents 20 μm for all images. (D) Quantification of anti-dpErk fluorescence intensity in leading-edge cells over time (see *Materials and Methods*). At all time points tested after wounding, dpErk intensity is significantly lower in both *Mmp1* and *A58>Mmp1-dsRNA* mutants relative to wild type ($p < 0.001$ for all mutant vs. wild-type comparisons) by Student's *t* test. Numbers on each bar indicate the number of cells measured. Error bars represent SEM.

lengths from the wound (compare Figure 7, B and F). Of importance, *egr* overexpression in the epidermis caused accelerated wound closure. Five hours postwounding, *A58>egr* wounds are significantly smaller than wild type (Figure 7, B, F, G, G″, H, H″, I, and J). To determine whether the accelerated wound closure is *Mmp1* dependent, we generated mutants that simultaneously overexpressed *egr* and knocked down *Mmp1* in the epidermis

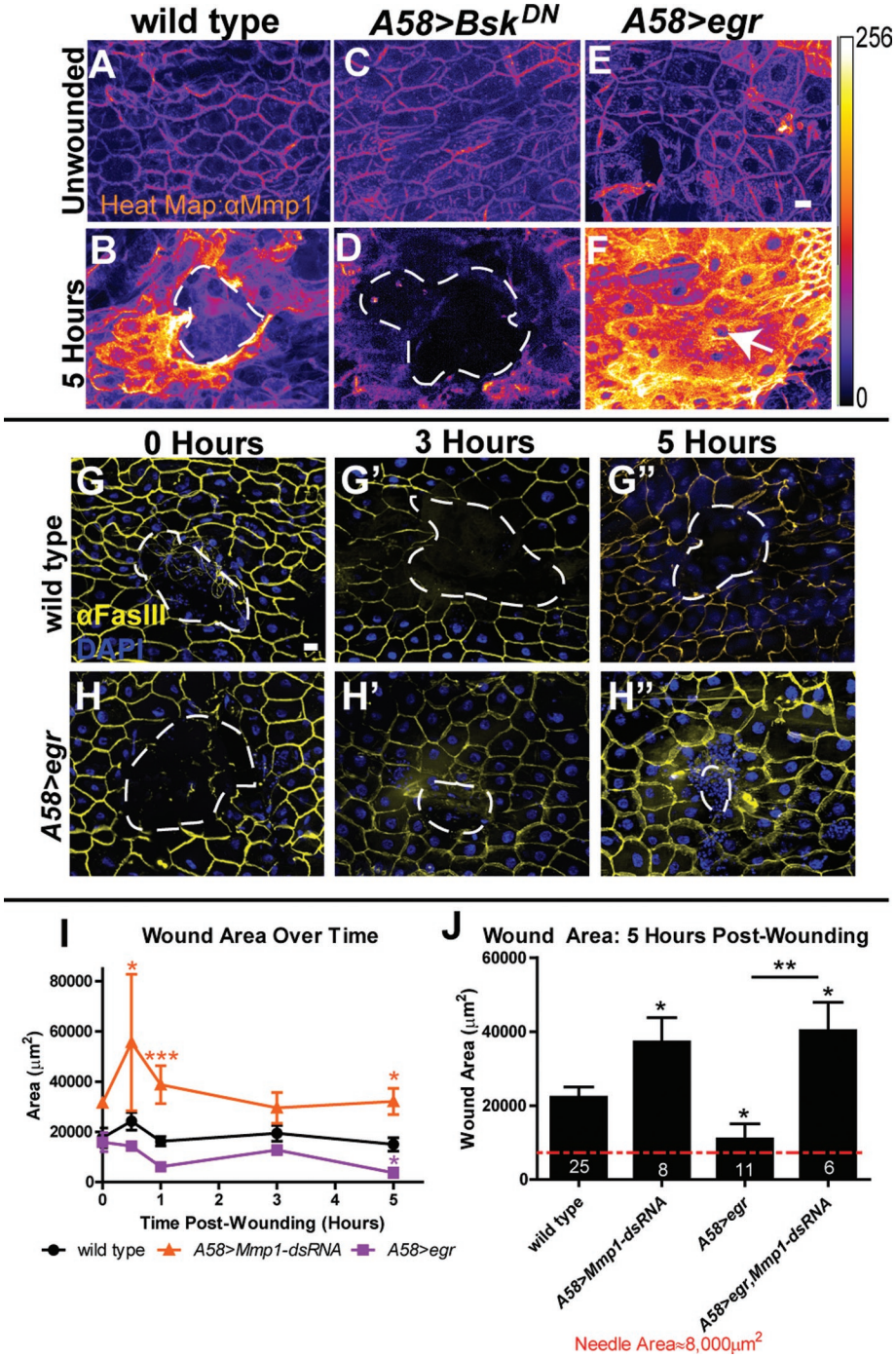


FIGURE 7: Mmp1 is positively regulated by JNK signaling during wound healing. (A–F) Heat map showing Mmp1 expression in the epidermis in unwounded condition (A, C, E) and 5 h postwounding (B, D, F) in the designated genotypes, pseudocolored based on pixel intensity (intensity scale shown on right). A white, dashed line (B, D) outlines the open wound beds. The white arrow (F) indicates the very small wound bed in *A58>egr* wounded epidermis. n ≥ 5 for each genotype. Scale bar in E represents 20 μm for A–F. (G, H) Images of wounds at 0 h (G, H), 3 h (G′, H′), and 5 h (G″, H″) postwounding in wild type (G–G″) and *A58>egr* (H–H″) labeled with FasIII (yellow) and DAPI (blue). White, dashed lines outline the wound bed. Scale bar in G represents 20 μm for G–H″. (I) Quantification of wound area over time in *A58>Mmp1-dsRNA* (orange line), wild type (black line), and *A58>egr* (purple line). *A58>Mmp1-dsRNA* wounds are significantly larger than wild-type wounds at 0.5 h ($p = 0.032$), 1 h ($p = 0.0005$), and 5 h ($p = 0.0027$) by Student's *t* test. *A58>egr* wounds are significantly smaller than wild-type wounds at 5 h ($p = 0.031$) by *t* test. There is no significant difference in wound area between mutants and wild type in initial wound area (0 h). Areas of three or more wounds were measured for each time point. (J) Wound area 5 h postwounding for the indicated genotypes. By *t* test, wounds in *A58>Mmp1-dsRNA* ($p = 0.021$), *A58>egr* ($p = 0.031$) and *A58>egr, Mmp1-dsRNA* ($p = 0.017$) are all significantly different from wild type. In addition, by *t* test, *A58>egr* wounds are significantly smaller than *A58>egr, Mmp1-dsRNA* ($p = 0.0024$) wounds at 5 h postwounding. There is no significant difference in wound area 5 h postwounding between *A58>Mmp1-dsRNA* and *A58>egr, Mmp1-dsRNA* mutants ($p = 0.77$) by *t* test. All error bars represent SEM.

(A58>*egr, Mmp1-dsRNA*). We found that by 5 h postwounding, not only was the average wound area in *A58>egr, Mmp1-dsRNA* mutants significantly larger than in both wild type and *A58>egr* alone (Figure 7I), but in addition the wound areas were similar between *A58>egr, Mmp1-dsRNA* compared with *A58>Mmp1-dsRNA* (Figure 7J). Taken together with the expression data, these results indicate that Mmp1 is downstream of and required for the accelerated healing function of egr. Although our data are consistent with the hypothesis that Mmp1 levels determine the rate of closure, it is also possible that other targets of egr signaling accelerate healing, and Mmp1 is simply a permissive factor. Unfortunately we could not test whether increased Mmp1 directly accelerates healing, because all animals ectopically expressing (GAL4-mediated) epidermal Mmp1 were lethal before third instar, even in the presence of GAL80 (data not shown). As a whole, our results demonstrate that the *Drosophila* secreted MMP—Mmp1—is upregulated in wounded epidermis, where it promotes epidermal reepithelialization, basement membrane repair, and wound signaling.

## DISCUSSION

To bypass the complexities of the large and redundant set of MMPs expressed in mammalian wounds, we used the simple model organism *Drosophila* to analyze MMP function in wound healing. We find that both *Mmp1*- and *Mmp2*-null mutants display not just delays in wound healing, but also a complete failure of reepithelialization. Of interest, wounding the double-*Mmp2 Mmp1* mutants identifies the first instance of MMP redundancy in *Drosophila*: the two MMPs are redundant for clotting, as the double mutants bleed out within a few hours after wounding. Thus both MMPs are required for reepithelialization, and either MMP is required for hemostasis. Focusing on the role of the secreted MMP, we find that *Mmp1* is required in the epidermis for reepithelialization and that *Mmp1* is required for cell elongation, reorganization of the actin cytoskeleton, repair of the basement membrane, and promotion of ERK signaling.

### Mmp1 promotes assembly and repair of basement membrane

Of the many defects observed in the *Mmp1*-mutant wounds, it is possible that the defects in the basement membrane are primary, with the other phenotypes as consequences. Not only do leading-edge cells fail to deposit collagen IV at the wound, but in addition even unwounded basement membrane appears abnormal with respect to collagen IV levels. These data lead to the surprising conclusion that a secreted MMP is required not for matrix degradation, but to promote matrix assembly. Although this may seem paradoxical, we envision MMPs contributing to ECM assembly by cleaving the existing basement membrane in order to insert new molecules, a step that may be required for matrix expansion as the animal grows. We note that the *MMP-14* (MT1-MMP) knockout mouse has weakened tendons, suggesting a precedent for MMPs in promoting extracellular matrix assembly (Holmbeck *et al.*, 1999), although the matrix of fibrillar collagen and basement membrane are very different.

The inability to deposit basement membrane could lead to severe consequences for wound healing. If the wound cannot repair the basement membrane, the cells could lack a scaffold to support cell migration, resulting in cell elongation failures and open wounds, as observed. It seems likely that the compromised basement membrane in the mutants is weaker than in wild type. The *Mmp1*-mutant wounds were much larger than wild-type wounds, suggesting that they gap open after puncture. The actin stress fibers observed in *Mmp1*-mutant wounds may simply be a compensatory mechanism for the weak basement membrane, as the tissue attempts to increase stability with actin cables, similar to the actin cable formed in *Drosophila* embryos closing wounds (Wood *et al.*, 2002). As cells migrate, they pull on their surrounding matrix, and a weak basement membrane may lack the resistance necessary for cell migration (Discher *et al.*, 2005; Kirmse *et al.*, 2011). In addition, we note that the Mmp1 epidermal samples are much more fragile during dissection than the wild-type controls, possibly because of weakened basement membranes.

### Mmp1 levels are regulated by JNK in response to wounding

Wound healing is a tightly regulated processes, involving the orchestration of several signaling cascades, including JNK signaling, which has been shown to be required for wound healing (Ramet *et al.*, 2002; Galko and Krasnow, 2004). MMPs have been shown to be regulated by JNK signaling in *Drosophila* during imaginal disk morphogenesis (Srivastava *et al.*, 2007), in *Drosophila* tumor models (Uhlirova and Bohmann, 2006), and in zebrafish during the inflammatory phase of wound healing (Zhang *et al.*, 2008). In addition, JNK regulation of MMPs has been observed in mammalian cell culture (Gum *et al.*, 1997). We find that the dramatic Mmp1 up-regulation in wounded epidermis depends on JNK signaling. However, in unwounded epidermis, Mmp1 is expressed independent of JNK signaling, suggesting that only inflammatory levels of Mmp1, but not homeostatic levels of Mmp1, are under JNK control. Animals misexpressing TNF (*eiger*) in the epidermis and hyperactivating JNK have dramatically increased Mmp1 expression after wounding, and they display accelerated reepithelialization. Of importance, this accelerated healing depends on *Mmp1*.

In mammals, *MMP-3, MMP-8, MMP-9,* and *MMP-13* knockout mice have defects in wound healing. Although all these are secreted MMPs, the wounding phenotypes observed in fly *Mmp1* mutants, which lack all secreted MMPs, are most similar to *MMP-9*$^{-/-}$ mice. These mice have delayed reepithelialization attributed to reduced mobility of their keratinocytes, which migrate more slowly ex vivo (Kyriakides *et al.*, 2009). Of interest, these mice also have abnormal deposition of collagen fibers. The main phenotypic difference between the *MMP-9*$^{-/-}$mice and the *Mmp1*-mutant flies is that the fly wounds do not heal at all. By taking advantage of the many genetic tools available for *Drosophila*, our data demonstrate that *Mmp1*, under the control of the JNK pathway, functions during reepithelialization in vivo to promote basement membrane deposition, cell elongation and migration, actin cytoskeletal reorganization, and ERK signaling.

## MATERIALS AND METHODS

### Fly lines

The following lines are described in Page-McCaw *et al.* (2003): *Mmp1*$^{2}$ and *Mmp2*$^{Df(2R)Uba1\text{-}Mmp2}$ (imprecise *P* excision alleles resulting in deletions of most or all of the coding region); *Mmp1*$^{Q112*}$ and *Mmp2*$^{W307*}$ (ethyl methanesulfonate [EMS]–induced nonsense alleles resulting in premature truncations); and *UAS-Timp* and *tubP-GAL4* (FlyBase [http://flybase.org/] ID FBtp0002651). The dominant-negative *Mmp1* line used was *UAS-Mmp1.f1*$^{E225A}$ (Zhang *et al.*, 2006; Glasheen *et al.*, 2009). Other fly lines used were as follows: *A58-Gal4* (M. Galko, University of Texas MD Anderson Cancer Center); *UAS-Bsk*$^{DN}$ (FlyBase ID FBti0074418) and *He-Gal4* (FlyBase ID FBti0064641), both from the Bloomington *Drosophila* Stock Center (Indiana University, Bloomington, IN); two lines of *UAS-Mmp1-dsRNA* (D. Bohmann and the Vienna *Drosophila* RNAi Center [Vienna, Austria] insertion 101505); *Vkg-GFP* $^{G205}$ (FlyTrap, Yale University, New Haven, CT); *UAS-egr* (M. Miura, University of Tokyo; shorter RB isoform (Igaki *et al.*, 2002); and *UAS-GFP-actin5C* (D. Kiehart, Duke University). *w*$^{1118}$ was used as wild type.

It has not been possible to perform rescue experiments using standard *Mmp1* constructs because *Mmp1* misexpression is lethal when widely expressed (even under permissive temperatures with a heat-shock promoter or under *GAL4/GAL80*$^{ts}$ control). As an alternative approach, a noncomplementation screen in an independent genetic background was performed in Page-McCaw *et al.* (2003) to identify new *Mmp1* alleles to show genetic specificity for *Mmp1*. Phenotypes in transheterozygotes (carrying a *P*-generated allele and an EMS allele) have been used to establish *Mmp1* specificity in previous reports (Page-McCaw *et al.*, 2003; Glasheen *et al.*, 2009, 2010), a strategy we employ in this study as well.

### Wounding assays

Third-instar larvae were impaled with a 0.1-mm steel needle (Fine Science Tools, Foster City, CA) on the dorsal side between segments A3 and A5 on molasses plates on ice. For pinch wounds, #5 dissecting forceps was used to gently pull/pinch the cuticle for ~5 s, without puncturing, on the dorsal side of third-instar larvae. Both assays were adapted from Galko and Krasnow (2004). After wounding, animals recovered on agar plates with access to wet yeast and water at 25°C.

### Dissection, fixation, and immunohistochemistry

To excise the epidermis, larvae were decapitated at the cerebral tracheal branch and filleted along the right lateral side, followed by removal of the posterior end at approximately segment A7. Dissections were done in phosphate-buffered saline (PBS) + 1% bovine serum albumin or directly in fixative. Tissue was pinned flat and fixed in PBS+ 4% formaldehyde at room temperature (RT) for 30 min. Fixed samples were washed and permeabilized in PBS + 0.2% Triton X-100, blocked in PBS + 5% goat serum + 0.02% $NaN_3$, incubated in primary antibody (diluted in PBS + 1% goat serum + 0.02% $NaN_3$) overnight at 4°C, washed and incubated in secondary antibodies for 1.5 h at RT in the dark, and mounted in Vectashield mounting

media with DAPI (Vector Laboratories, Burlingame, CA). Anti–Mmp1 catalytic domain (a 1:1:1 cocktail of mouse monoclonal immunoglobulin G1 [IgG1] antibodies 3B8, 5H7, and 23G, generated by Page-McCaw *et al.*, 2003, and obtained from the Developmental Studies Hybridoma Bank [DSHB; University of Iowa, Iowa City, IA]), was used at 1:100. Anti-FasIII (a mouse monoclonal IgG2a from the DSHB) was used at 1:10. Rabbit anti-GFP (Molecular Probes, Invitrogen, Carlsbad, CA) was preabsorbed against larval epidermis and used at 1:100. Mouse anti–integrin-βPS (a monoclonal IgG2b from DSHB) was used at 1:10. Mouse monoclonal IgG1 anti–diphosphorylated ERK 1 and 2 (Sigma-Aldrich, St. Louis, MO) was used at 1:100. Mouse monoclonal anti–collagen IV (gift of Lisa and John Fessler, University of California, Los Angeles) was used at 1:25. Cy3- or fluorescein isothiocyanate (FITC)–labeled goat anti–mouse IgG1 (Jackson ImmunoResearch Laboratories, West Grove, PA), DyeLight649-labeled goat anti–mouse IgG2a (Jackson ImmunoResearch Laboratories), Cy3-labeled goat anti-mouse (Jackson ImmunoResearch), and FITC-labeled donkey anti-rabbit (Jackson ImmunoResearch Laboratories) were all used at 1:300.

### Microscopy

Optical sectioning was performed with a Zeiss Apotome mounted on an Axio imager Z1 or M2, with the following objectives: 20×/0.8 Plan-Apochromat, 40×/1.3 oil EC Plan-NeoFluar, or 63×/1.4 oil Plan-Apochromat. Fluorescence images were acquired with an AxioCam MRm (Zeiss, Thornwood, NY) camera paired with AxioVision 4.8 (Zeiss). Z-stacks were compressed into two-dimensional projections using the Orthoview function in AxioVision. All images were exported from their acquisition programs as 16-bit, grayscale, TIFF files for postprocessing in Photoshop CS4 (Adobe, San Jose, CA) or ImageJ, version 1.43u (National Institutes of Health, Bethesda, MD).

### Wound measurements

Closure and wound area were assessed based on the presence of both FasIII staining at cell borders and epidermal polyploid nuclei as stained with DAPI. To calculate wound area, the outline tool in AxioVision was used to manually outline the wound edge. This feature automatically calculates the area of the outlined region using image acquisition specifications. In Figure 1, E and F, the wounded animals are as follows. Wild type (n = 19): $w^{1118}$. *Mmp1* (n = 6): 4 $Mmp1^{Q112*/2}$ and 2 $Mmp1^{2}$. *Mmp2* (n = 7): 4 $Mmp2^{W307*/Df(2R)Uba1\text{-}Mmp2}$ and 3 $Mmp2^{W307*}$. *A58>Timp* (n = 5). Student's *t* tests were performed with the analysis tools available in GraphPad Prism, version 5.01 (GraphPad Software, La Jolla, CA), to compare mutant and wild-type wound area within each time point.

To measure aspect ratios (Figure 5 and Supplemental S3), wounded epidermal samples were fixed at various times post-wounding (0 h is immediately after wounding) and stained for FasIII and DAPI. X-Y projections of wounds were generated from optical sections taken at 20×. On each leading-edge cell a line was drawn manually with ImageJ on the longest axis determined by FasIII staining, and then the longest perpendicular axis was drawn. The ImageJ measurement tool measured the lines, and aspect ratios were calculated in Excel (Microsoft, Redmond, WA). Because this method ignores cell orientation, the long axis was used as the numerator, so that the smallest possible ratio was 1.0. Only cells with FasIII on all edges were measured. We used n ≥ 29 cells from three different animals for each column. *Mmp1* was the transheterozygous $Mmp1^{Q112*/2}$. The mean aspect ratio for each genotype at each time point was calculated and graphed using GraphPad Prism, version 5.01. Error bars represent SEM. Student's *t* test was used to determine the statistical significance between pairs of columns.

### Expression analysis

To generate heat maps of pixel intensity from fluorescence images, single-channel, 16-bit grayscale two-dimensional projection Z-stacks were converted to 8-bit images in ImageJ, version 1.43u. The "fire" look-up table was then applied to the image to pseudocolor pixels based on intensity, with white = 256 and dark navy blue = 0.

To measure relative dpERK expression between genotypes over time, two-dimensional projection images were opened in ImageJ, and the ellipse tool was used to mark nuclei at the leading edge of the wound based on DAPI staining and anti-FasIII expression, while the dpERK channel was hidden. The multimeasure tool was then used to calculate an integrated intensity density for each region of interest (representing each nucleus) for the dpERK channel. Each integrated density value was imported into GraphPad Prism, version 5.01, where GraphPad Prism analysis tools were used to perform Student's *t* test to compare mutant intensity to wild-type intensity at each time point and to compare wild-type wounded intensity to wild-type unwounded intensity at each time point.

For Vkg-GFP intensity analysis in unwounded tissue, X-Y images of Vkg-GFP taken at 63× during seven blindly scored, independent trials were opened in ImageJ and automatically sized to 9.25 in. × 6.93 in. A 1-in.$^2$ square grid was applied to the image, and integrated density was calculated within each square using the ImageJ measure tool. Squares that contained only basement membrane were measured; squares that contained folds in the tissue or ECM from other tissue types were excluded. All intensity measurements were imported in an Excel spreadsheet, and the average pixel intensity for each sample (each animal) was calculated along with the overall average intensity for each genotype within each experimental replicate. To calculate relative expression intensity between *Mmp1* mutants and wild type, the ratio of mutant versus wild-type intensity was calculated for each sample within experimental replicate. The negative inverse was calculated for all ratios <1. Ratios for each mutant and wild-type sample were imported in GraphPad Prism and plotted on a box-and-whiskers plot, with wild-type ranging from –1 to 1. Student's *t* test was used to assess the differences between genotypes. A similar method was used to quantify anti–collagen IV staining intensity, except that the grid squares were ½ in.$^2$.

### Western blots

Third-instar larvae (one to three *Vkg-GFP/CyO* larvae or two to five *Vkg-GFP* $Mmp1^{2}/Mmp1^{Q112*}$ larvae) were homogenized in 30 µl of 2× Laemmli buffer with mini–complete protease inhibitors (Roche, Indianapolis, IN). A 20-µl amount of each lysate was loaded in each lane of a 4–15% Tris-glycine PAGE gradient gel (Bio-Rad, Hercules, CA). Blots were washed in PBS + 0.1% Tween-20, blocked in Odyssey Blocking Buffer (Bio-Rad), and probed with rabbit anti-GFP (Molecular Probes) used at 1:1000 or mouse anti-actin (Abcam, Cambridge, MA) used at 1:5000 overnight at 4°C. Secondary antibody incubations were 1 h at RT with goat anti-mouse labeled with IRdye800 (LI-COR Biosciences, Lincoln, NE) at 1:7500 or donkey anti-rabbit tagged with IRDye680 (LI-COR Biosciences) at 1:5000, followed by developing with the Odyssey Infrared Imaging System (LI-COR Biosciences). Integrated fluorescence intensity was calculated for the top bands (shown in Figure 4K) using ImageJ, version 1.43u, as these had no corresponding background bands in non–GFP-containing wild-type lanes; the intensities of these bands were summed to find total expression. Expression was normalized against integrated fluorescence intensity of the actin loading control. Fold change of anti-GFP expression in *Mmp1* mutants was calculated relative to that in wild type. No statistically significant difference was found between *Mmp1* mutants and wild type over three independent trials.

For the *Mmp1-dsRNA*–knockdown efficiency blots (Supplemental Figure S2), third-instar larvae (2 *Tub>Mmp1-dsRNA* of both the DB line and the VDRC line, 4 $Mmp1^2$, or 2 *Tub-Gal4*) were homogenized in 30 µl of 2× Laemmli buffer. A 20-µl amount of each lysate was loaded in each lane of a 10% Tris-glycine PAGE gel (Bio-Rad). Blots were washed in PBS + 0.1% Tween-20, blocked in Odyssey Blocking Buffer (Bio-Rad), and probed overnight at 4°C with 1:1:1 cocktail of monoclonal mouse anti-Mmp1 antibodies 3B8, 5H7, and 3A6 (DSHB) used at 1:100 and with rat anti–α-tubulin (AbD Serotec, Raleigh, NC) used at 1:5000. Secondary antibody incubations were at RT for 1 h in donkey anti-mouse labeled with IRdye800 at 1:5000 or donkey anti-rat tagged with IRDye680 at 1:7500, followed by developing with the Odyssey Infrared Imaging System. Three independent trials were performed, and results were quantified following the methods outlined for the Vkg-GFP blots, with Mmp1 expression normalized against α-tubulin expression within each lane. Normalized intensity values were imported into GraphPad Prism, version 5.01, where the mean and SEM were plotted for each genotype and the p value was calculated by a Student's *t* test comparing each mutant/knockdown expression level to wild type.

## ACKNOWLEDGMENTS

We thank Patrick Page-McCaw for the early suggestion of wound assays, Laura Lee for extracellular matrix observations, Sarah Broderick for many suggestions and for reading several drafts of the manuscript, and Kimi LaFever for assistance with dpERK staining. We thank Heather Broihier for comments on the manuscript. We thank M. Galko, D. Bohmann, D. Kiehart, M. Miura, and the Bloomington *Drosophila* Stock Center for fly stocks and L. and J. Fessler and the Developmental Studies Hybridoma Bank for antibodies. This work was supported by National Institutes of Health Grant R01 GM073883 to A.P.M.

## REFERENCES

Beaucher M, Hersperger E, Page-McCaw A, Shearn A (2007). Metastatic ability of *Drosophila* tumors depends on MMP activity. Dev Biol 303, 625–634.

Bergers G *et al.* (2000). Matrix metalloproteinase-9 triggers the angiogenic switch during carcinogenesis. Nat Cell Biol 2, 737–744.

Brenner DA, O'Hara M, Angel P, Chojkier M, Karin M (1989). Prolonged activation of jun and collagenase genes by tumour necrosis factor-alpha. Nature 337, 661–663.

Bullard KM, Lund L, Mudgett JS, Mellin TN, Hunt TK, Murphy B, Ronan J, Werb Z, Banda MJ (1999). Impaired wound contraction in stromelysin-1-deficient mice. Ann Surg 230, 260–265.

Discher DE, Janmey P, Wang Y-L (2005). Tissue cells feel and respond to the stiffness of their substrate. Science 310, 1139–1143.

Doehn U *et al.* (2009). RSK is a principal effector of the RAS-ERK pathway for eliciting a coordinate promotile/invasive gene program and phenotype in epithelial cells. Mol Cell 35, 511–522.

Egeblad M, Werb Z (2002). New functions for the matrix metalloproteinases in cancer progression. Nat Rev Cancer 2, 161–174.

Gabay L, Seger R, Shilo BZ (1997). In situ activation pattern of *Drosophila* EGF receptor pathway during development. Science 277, 1103–1106.

Galko MJ, Krasnow MA (2004). Cellular and genetic analysis of wound healing in *Drosophila* larvae. PLoS Biol 2, E239.

Gearing A *et al.* (1995). Matrix metalloproteinases and processing of pro-TNF-alpha. J Leukocyte Biol 57, 774–777.

Gill SE, Parks WC (2008). Metalloproteinases and their inhibitors: regulators of wound healing. Int J Biochem Cell Biol 40, 1334–1347.

Glasheen BM, Kabra AT, Page-McCaw A (2009). Distinct functions for the catalytic and hemopexin domains of a *Drosophila* matrix metalloproteinase. Proc Natl Acad Sci USA 106, 2659–2664.

Glasheen BM, Robbins RM, Piette C, Beitel GJ, Page-McCaw A (2010). A matrix metalloproteinase mediates airway remodeling in *Drosophila*. Dev Biol 344, 772–783.

Godenschwege TA, Pohar N, Buchner S, Buchner E (2000). Inflated wings, tissue autolysis and early death in tissue inhibitor of metalloproteinases mutants of *Drosophila*. Eur J Cell Biol 79, 495–501.

Goldberg SR, Diegelmann RF (2010). Wound healing primer. Surg Clin North Am 90, 1133–1146.

Gomis-Ruth FX *et al.* (1997). Mechanism of inhibition of the human matrix metalloproteinase stromelysin-1 by TIMP-1. Nature 389, 77–81.

Gum R, Wang H, Lengyel E, Juarez J, Boyd D (1997). Regulation of 92 kDa type IV collagenase expression by the jun aminoterminal kinase- and the extracellular signal-regulated kinase-dependent signaling cascades. Oncogene 14, 1481–1493.

Gurtner GC, Werner S, Barrandon Y, Longaker MT (2008). Wound repair and regeneration. Nature 453, 314–321.

Gutierrez-Fernandez A *et al.* (2007). Increased inflammation delays wound healing in mice deficient in collagenase-2 (MMP-8). FASEB J 21, 2580–2591.

Hattori N, Mochizuki S, Kishi K, Nakajima T, Takaishi H, D'Armiento J, Okada Y (2009). MMP-13 plays a role in keratinocyte migration, angiogenesis, and contraction in mouse skin wound healing. Am J Pathol 175, 533–546.

Helman A, Paroush Z (2010). Detection of RTK pathway activation in *Drosophila* using anti-dpERK immunofluorescence staining. Methods Mol Biol 661, 401–408.

Holmbeck K *et al.* (1999). MT1-MMP-deficient mice develop dwarfism, osteopenia, arthritis, and connective tissue disease due to inadequate collagen turnover. Cell 99, 81–92.

Hynes RO, Zhao Q (2000). The evolution of cell adhesion. J Cell Biol 150, F89–F96.

Igaki T, Kanda H, Yamamoto-Goto Y, Kanuka H, Kuranaga E, Aigaki T, Miura M (2002). Eiger, a TNF superfamily ligand that triggers the *Drosophila* JNK pathway. EMBO J 21, 3009–3018.

Igaki T, Pastor-Pareja JC, Aonuma H, Miura M, Xu T (2009). Intrinsic tumor suppression and epithelial maintenance by endocytic activation of Eiger/TNF signaling in *Drosophila*. Dev Cell 16, 458–465.

Kirmse R, Otto H, Ludwig T (2011). Interdependency of cell adhesion, force generation and extracellular proteolysis in matrix remodeling. J Cell Sci 124, 1857–1866.

Koshikawa N, Schenk S, Moeckel G, Sharabi A, Miyazaki K, Gardner H, Zent R, Quaranta V (2004). Proteolytic processing of laminin-5 by MT1-MMP in tissues and its effects on epithelial cell morphology. FASEB J 18, 364–366.

Kyriakides TR, Wulsin D, Skokos EA, Fleckman P, Pirrone A, Shipley JM, Senior RM, Bornstein P (2009). Mice that lack matrix metalloproteinase-9 display delayed wound healing associated with delayed reepithelization and disordered collagen fibrillogenesis. Matrix Biol 28, 65–73.

Levi E, Fridman R, Miao HQ, Ma YS, Yayon A, Vlodavsky I (1996). Matrix metalloproteinase 2 releases active soluble ectodomain of fibroblast growth factor receptor 1. Proc Natl Acad Sci USA 93, 7069–7074.

Li Q, Park PW, Wilson CL, Parks WC (2002). Matrilysin shedding of syndecan-1 regulates chemokine mobilization and transepithelial efflux of neutrophils in acute lung injury. Cell 111, 635–646.

Llano E, Adam G, Pendas AM, Quesada V, Sanchez LM, Santamaria I, Noselli S, Lopez-Otin C (2002). Structural and enzymatic characterization of *Drosophila* Dm2-MMP, a membrane-bound matrix metalloproteinase with tissue-specific expression. J Biol Chem 277, 23321–23329.

Llano E, Pendas AM, Aza-Blanc P, Kornberg TB, Lopez-Otin C (2000). Dm1-MMP, a matrix metalloproteinase from *Drosophila* with a potential role in extracellular matrix remodeling during neural development. J Biol Chem 275, 35978–35985.

Martinez Arias A (1993). Bate M, Martinez Arias A (1993). Development and patterning of the larval epidermis of *Drosophila*. The Development of *Drosophila melanogaster* 1, Plainview, NY: Cold Spring Harbor Laboratory Press, 517–608.

Matsubayashi Y, Ebisuya M, Honjoh S, Nishida E (2004). ERK activation propagates in epithelial cell sheets and regulates their migration during wound healing. Curr Biol 14, 731–735.

Menke NB, Ward KR, Witten TM, Bonchev DG, Diegelmann RF (2007). Impaired wound healing. Clin Dermatol 25, 19–25.

Mogilner A, Keren K (2009). The shape of motile cells. Curr Biol 19, R762–R771.

Morin X, Daneman R, Zavortink M, Chia W (2001). A protein trap strategy to detect GFP-tagged proteins expressed from their endogenous loci in *Drosophila*. Proc Natl Acad Sci USA 98, 15050–15055.

Mott JD, Werb Z (2004). Regulation of matrix biology by matrix metalloproteinases. Curr Opin Cell Biol 16, 558–564.

Murray MJ, Fessler LI, Palka J (1995). Changing distributions of extracellular matrix components during early wing morphogenesis in *Drosophila*. Dev Biol 168, 150–165.
Noselli S (1998). JNK signaling and morphogenesis in *Drosophila*. Trends Genet 14, 33–38.
Page-McCaw A, Ewald AJ, Werb Z (2007). Matrix metalloproteinases and the regulation of tissue remodelling. Nat Rev Mol Cell Biol 8, 221–233.
Page-McCaw A, Serano J, Sante JM, Rubin GM (2003). *Drosophila* matrix metalloproteinases are required for tissue remodeling, but not embryonic development. Dev Cell 4, 95–106.
Pal-Ghosh S, Blanco T, Tadvalkar G, Pajoohesh-Ganji A, Parthasarathy A, Zieske JD, Stepp MA (2011). MMP9 cleavage of the β4 integrin ectodomain leads to recurrent epithelial erosions in mice. J Cell Sci 124, 2666–2675.
Parks WC, Wilson CL, Lopez-Boado YS (2004). Matrix metalloproteinases as modulators of inflammation and innate immunity. Nat Rev Immunol 4, 617–629.
Pastor-Pareja JC, Xu T (2011). Shaping cells and organs in *Drosophila* by opposing roles of fat body-secreted collagen iv and perlecan. Dev Cell 21, 245–256.
Ramet M, Lanot R, Zachary D, Manfruelli P (2002). JNK signaling pathway is required for efficient wound healing in *Drosophila*. Dev Biol 241, 145–156.
Rebustini IT, Myers C, Lassiter KS, Surmak A, Szabova L, Holmbeck K, Pedchenko V, Hudson BG, Hoffman MP (2009). MT2-MMP-dependent release of collagen IV NC1 domains regulates submandibular gland branching morphogenesis. Dev Cell 17, 482–493.
Schultz GS, Wysocki A (2009). Interactions between extracellular matrix and growth factors in wound healing. Wound Repair Regen 17, 153–162.
Shaw TJ, Martin P (2009). Wound repair at a glance. J Cell Sci 122, 3209–3213.
Singer AJ, Clark RA (1999). Cutaneous wound healing. N Engl J Med 341, 738–746.
Smith AV, Orr-Weaver TL (1991). The regulation of the cell cycle during *Drosophila* embryogenesis: the transition to polyteny. Development 112, 997–1008.
Srivastava A, Pastor-Pareja JC, Igaki T, Pagliarini R, Xu T (2007). Basement membrane remodeling is essential for *Drosophila* disc eversion and tumor invasion. Proc Natl Acad Sci USA 104, 2721–2726.
Suzuki M, Raab G, Moses MA, Fernandez CA, Klagsbrun M (1997). Matrix metalloproteinase-3 releases active heparin-binding EGF-like growth factor by cleavage at a specific juxtamembrane site. J Biol Chem 272, 31730–31737.
Tholozan FMD, Gribbon C, Li Z, Goldberg MW, Prescott AR, McKie N, Quinlan RA (2007). FGF-2 release from the lens capsule by MMP-2 maintains lens epithelial cell viability. Mol Biol Cell 18, 4222–4231.
Uhlirova M, Bohmann D (2006). JNK- and Fos-regulated Mmp1 expression cooperates with Ras to induce invasive tumors in *Drosophila*. EMBO J 25, 5294–5304.
Vaisar T, Kassim SY, Gomez IG, Green PS, Hargarten S, Gough PJ, Parks WC, Wilson CL, Raines EW, Heinecke JW (2009). MMP-9 sheds the beta2 integrin subunit (CD18) from macrophages. Mol Cell Proteomics 8, 1044–1060.
Verkhusha VV, Tsukita S, Oda H (1999). Actin dynamics in lamellipodia of migrating border cells in the *Drosophila* ovary revealed by a GFP-actin fusion protein. FEBS Lett 445, 395–401.
Wei S, Xie Z, Filenova E, Brew K (2003). *Drosophila* TIMP is a potent inhibitor of MMPs and TACE: similarities in structure and function to TIMP-3. Biochemistry 42, 12200–12207.
Wood W, Jacinto A, Grose R, Woolner S, Gale J, Wilson C, Martin P (2002). Wound healing recapitulates morphogenesis in *Drosophila* embryos. Nat Cell Biol 4, 907–912.
Wu Y, Brock AR, Wang Y, Fujitani K, Ueda R, Galko MJ (2009). A blood-borne PDGF/VEGF-like ligand initiates wound-induced epidermal cell migration in *Drosophila* larvae. Curr Biol 19, 1473–1477.
Yasothornsrikul S, Davis WJ, Cramer G, Kimbrell DA, Dearolf CR (1997). viking: identification and characterization of a second type IV collagen in *Drosophila*. Gene 198, 17–25.
Yu Q, Stamenkovic I (2000). Cell surface-localized matrix metalloproteinase-9 proteolytically activates TGF-beta and promotes tumor invasion and angiogenesis. Genes Dev 14, 163–176.
Zhang S, Dailey GM, Kwan E, Glasheen BM, Sroga GE, Page-McCaw A (2006). An MMP liberates the Ninjurin A ectodomain to signal a loss of cell adhesion. Genes Dev 20, 1899–1910.
Zhang Y *et al.* (2008). In vivo interstitial migration of primitive macrophages mediated by JNK-matrix metalloproteinase 13 signaling in response to acute injury. J Immunol 181, 2155–2164.